On Cabbeling and Thermobaricity in the Surface Mixed Layer

K. D. STEWART

Research School of Earth Sciences and Australian Research Council Centre of Excellence for Climate System Science, Australian National University, Canberra, Australian Capital Territory, Australia

T. W. N. HAINE

Department of Earth and Planetary Sciences, The Johns Hopkins University, Baltimore, Maryland

A. MCC. HOGG

Research School of Earth Sciences and Australian Research Council Centre of Excellence for Climate System Science, Australian National University, Canberra, Australian Capital Territory, Australia

F. ROQUET

Department of Meteorology, Stockholm University, Stockholm, Sweden

(Manuscript received 12 February 2017, in final form 18 April 2017)

ABSTRACT

The surface mixed layer (ML) governs atmosphere–ocean fluxes, and thereby affects Earth's climate. Accurate representation of ML processes in ocean models remains a challenge, however. The $O(100)$ m deep ML exhibits substantial horizontal thermohaline gradients, despite being near-homogenous vertically, making it an ideal location for processes that result from the nonlinearity of the equation of state, such as cabbeling and thermobaricity. Traditional approaches to investigate these processes focus on their roles in interior water-mass transformation and are ill suited to examine their influence on the ML. However, given the climatic significance of the ML, quantifying the extent to which cabbeling and thermobaricity influence the ML density field offers insight into improving ML representations in ocean models. A recent simplified equation of state of seawater allows the local effects of cabbeling and thermobaric processes in the ML to be expressed analytically as functions of the local temperature gradient and ML depth. These simplified expressions are used to estimate the extent to which cabbeling and thermobaricity contribute to local ML density differences. These estimates compare well with values calculated directly using the complete nonlinear equation of state. Cabbeling and thermobaricity predominantly influence the ML density field poleward of 30°. Mixed layer thermobaricity is basin-scale and winter intensified, while ML cabbeling is perennial and localized to intense, zonally coherent regions associated with strong temperature fronts, such as the Antarctic Circumpolar Current and the Kuroshio and Gulf Stream Extensions. For latitudes between 40° and 50° in both hemispheres, the zonally averaged effects of ML cabbeling and ML thermobaricity can contribute on the order of 10% of the local ML density difference.

1. Introduction

The ocean surface mixed layer (ML) mediates the exchange of heat, freshwater, and CO_2 between the atmosphere and ocean, thereby playing a major role in Earth's climate. The dynamics of the ML, along with their driving mechanisms (e.g., winds, tides, and surface buoyancy fluxes), span a wide range of time and length scales and tend to vertically homogenize the ML and maintain its characteristically weak stratification. While being well-mixed vertically, regions of the ML exhibit substantial horizontal gradients in temperature and salinity, especially in the transition zone oceans between alpha and beta oceans[1]

Corresponding author: K. D. Stewart, kial.stewart@anu.edu.au

[1] Alpha and beta oceans are regions where the stratification is permanently set by heat and salt, respectively, and are separated by transition zone oceans where the stratification is seasonally or intermittently set by heat or salt.

DOI: 10.1175/JPO-D-17-0025.1

(e.g., Carmack 2007; Stewart and Haine 2016). These thermohaline gradients are often density compensating, resulting in small horizontal gradients of density for large gradients of temperature and salinity. Although these local horizontal density gradients within the ML are relatively small compared with the basin-scale density differences, they can generate local convective instabilities and maintain overturning circulations, thereby enhancing atmosphere–ocean exchanges (e.g., Haine and Marshall 1998). Dynamics associated with nonlinearities in the equation of state of seawater can further increase these horizontal density gradients in the ML and enhance these ML exchanges and overturnings.

The density of seawater depends on its temperature, salinity, and pressure and is most accurately described by the International Thermodynamic Equation of Seawater–2010 (TEOS-10; IOC et al. 2010). Roquet et al. (2015b) demonstrate that for many oceanographic applications the TEOS-10 can be approximated by a relatively simple polynomial. This polynomial expression for the equation of state is useful for isolating the specific nonlinear contributions to the density of seawater and gauging their relative influence on the ocean state. The two nonlinear terms that have the largest influence on seawater density, and subsequently the ocean circulation, are those relating to cabbeling and thermobaricity (e.g., McDougall 1987; Nycander et al. 2015). Put simply, cabbeling relates to the phenomenon that the mixture of water masses of different temperatures is denser than the average of the source densities, and thermobaricity relates to the fact that the compressibility of seawater is inversely related to its temperature, resulting in cold water being more compressible than warm water (e.g., see Fig. 1 of Stewart and Haine 2016).

Studies investigating the oceanic effects of cabbeling and thermobaricity have focused on the tendency to induce a diapycnal advection (i.e., water-mass transformation) across neutral surfaces via isoneutral mixing (e.g., McDougall 1987; Klocker and McDougall 2010; Groeskamp et al. 2016). In this framework, cabbeling occurs in regions with large isoneutral temperature gradients and thermobaricity in regions with both large isoneutral temperature gradients and isoneutral pressure gradients (i.e., inclined neutral surfaces). Importantly, by these definitions, both cabbeling and thermobaricity arise from the same physical process (isoneutral mixing) and induce the same physical result (diapycnal advection) and are thus directly comparable. In the ML, despite the neutral surfaces being near-vertical and the large isoneutral mixing (that maintains the vertical homogeneity of ML water properties), the isoneutral temperature gradients are small, meaning that the water-mass transformation by cabbeling and thermobaricity in the ML is negligible.

Nevertheless, the underlying thermodynamics of cabbeling and thermobaricity can still influence the ML density field. For example, consider a north–south ocean section where the surface thermohaline gradients are density compensating, such that the horizontal surface density gradient is small (Fig. 1). Because of the temperature-dependent compressibility of seawater (the thermodynamical process responsible for thermobaricity), the cooler waters in the south are more compressible than the warmer waters in the north, meaning that as the surface temperatures and salinities penetrate vertically through the ML (either by diffusion or advection) to greater pressures the horizontal density difference increases (Fig. 1, left), with the cooler waters becoming more dense than the warmer waters. Alternatively, if this ocean section mixes horizontally, the density of the product water mass is greater than the mean of the source densities due to the same thermodynamics responsible for cabbeling (Fig. 1, right).

It is important to note that, unlike the McDougall (1987) notion of cabbeling and thermobaricity, these processes in the ML manifest under different circumstances. Here, the ML cabbeling effect requires the horizontal mixing of water masses with different temperatures and salinities, while the ML thermobaric effect requires a vertical penetration (advection or diffusion) of surface temperatures and salinities to greater pressure without requiring horizontal mixing. Both of these circumstances (horizontal mixing and vertical penetration) are ubiquitous throughout the ML, and we therefore expect these ML cabbeling and ML thermobaric processes to have an influence on the ML density field. Additionally, the physical results of these ML processes differ; ML cabbeling results in product water that is relatively denser than the average density of the source waters, while ML thermobaricity results in horizontal density differences increasing with depth through the ML. One must be mindful of this difference when directly comparing these ML processes. Nevertheless, the effects of ML cabbeling and ML thermobaricity can be expressed in terms of the increase in horizontal density difference within the ML, thereby providing a useful means to examine the relative extent and distributions of these ML processes.

Here, we investigate the influence of cabbeling and thermobaricity in the ML. We develop an analytical expression from the Roquet et al. (2015a) simplified "realistic"[2] equation of state that is used to identify

[2] The Roquet et al. (2015a) polynomial approximation for the equation of state of seawater is referred to as "realistic" because it captures to first order the nonlinear effects of the complete equation of state.

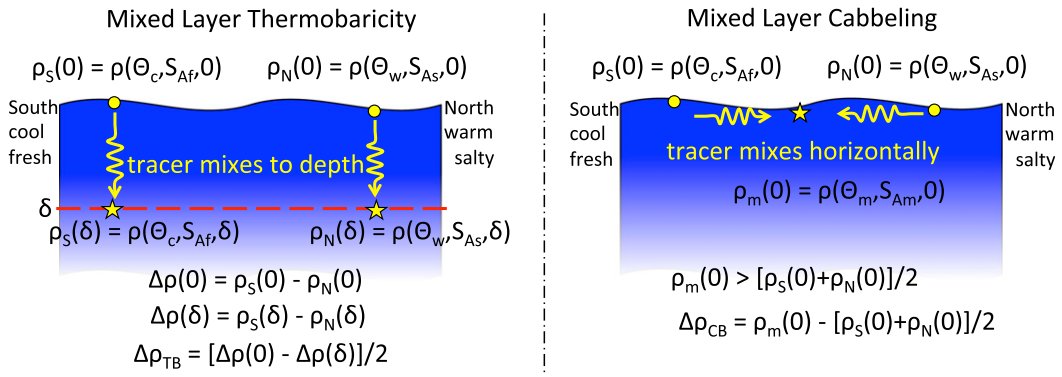

FIG. 1. A schematic depicting the consequences of ML thermobaricity and ML cabbeling. Consider two parcels of surface water with different temperatures and salinities, such that the southern parcel is relatively cooler and fresher than the northern parcel. (left) The horizontal density difference between these two parcels at the surface is $\Delta\rho(0) = \rho_S(0) - \rho_N(0)$. ML dynamics transport the cool/fresh and warm/salty tracers from the ocean surface to the bottom of the ML, $Z = \delta$, where the horizontal density difference is $\Delta\rho(\delta)$. The compressibility of the water parcels is an inverse function of its temperature, so that the relatively cooler southern water is more compressible than the northern water, resulting in $\Delta\rho(0) \neq \Delta\rho(\delta)$. Thus, averaged over the depth of the ML, the thermobaric contribution to the horizontal ML density difference is $\Delta\rho_T = [\Delta\rho(0) - \Delta\rho(\delta)]/2$. (right) If the two parcels mix horizontally, the resultant temperature and salinity is the average of the two parcels. The resultant density $\rho_m(0)$ is greater than the average density of the two parcels, however, due to cabbeling processes. The extent to which cabbeling processes can densify the ML is expressed as the difference between the mixed water density and the average of the initial water densities, $\Delta\rho_C = \rho_m(0) - [\rho_S(0) + \rho_N(0)]/2$.

regions where the effects of cabbeling and thermobaricity occur in the ML (section 2). This methodology uses the local horizontal temperature differences and ML depths from the Monthly Isopycnal/Mixed-Layer Ocean Climatology (MIMOC) product (section 3; Schmidtko et al. 2013) to estimate upper bounds for the local density difference increase due to ML cabbeling and ML thermobaricity. The estimates calculated with the Roquet et al. (2015a) simplified expression are compared with values computed from the full TEOS-10 and found to be in good agreement (section 4). We find these nonlinear processes occur in the ML predominantly poleward of 30°. Thermobaricity in the ML is basin scale, winter intensified, and generally has a stronger influence than ML cabbeling processes, which is localized to zonally coherent regions and perennial. Mixed layer cabbeling and ML thermobaricity account for upward of 10% of the local ML density differences in the subpolar and extratropical oceans.

2. Theory

Seawater density ρ (kg m^{-3}) is given by the TEOS-10 (IOC et al. 2010) as a function of Conservative Temperature Θ (°C), Absolute Salinity S_A (g kg^{-1}), and pressure p (Pa):

$$\rho^{t10} = \rho(\Theta, S_A, p), \tag{1}$$

where the superscript $t10$ indicates the term is calculated with the TEOS-10. For convenience, hereinafter we refer to Conservative Temperature and Absolute Salinity simply as "temperature" and "salinity," respectively. Following Roquet et al. (2015a), for the purposes of the simplified equation of state and the analysis presented here, it is sufficient to use the geopotential depth Z (m) in place of pressure with $Z = p \times 1\,\mathrm{m\,dbar^{-1}}$. Additionally, a density anomaly variable ρ' is defined as

$$\rho = \overline{\rho}(z) - \rho', \tag{2}$$

with $\overline{\rho}(z)$ serving as the reference density for the depth z. Employing ρ' focuses the investigation on the dynamical effects alone. Equation (17) of Roquet et al. (2015a) gives the simplest, yet realistic, equation of state of seawater as

$$\rho' = -\frac{C_b}{2}(\Theta - \Theta_0)^2 - T_h Z\Theta + b_0 S_A, \tag{3}$$

with

$$C_b = 0.011\,\mathrm{kg m^{-3} K^{-2}},$$
$$T_h = 2.5 \times 10^{-5}\,\mathrm{kg m^{-4} K^{-1}},$$
$$b_0 = 0.77\,\mathrm{kg m^{-3}(g kg^{-1})}, \quad \text{and}$$
$$\Theta_0 = -4.5°\mathrm{C}.$$

Here, C_b and T_h are the effective cabbeling and thermobaricity coefficients, respectively; b_0 is a constant

haline contraction coefficient; and Θ_0 is the temperature at which the surface thermal expansion coefficient is zero.

From the examples described in section 1, consider the two regions of Fig. 1. The south is relatively cold (Θ_c) and fresh (S_{Af}), and the north is relatively warm (Θ_w) and salty (S_{As}). The respective density anomalies of the southern and northern regions at geopotential depth Z are

$$\rho'_S(Z) = -\frac{C_b}{2}(\Theta_c - \Theta_0)^2 - T_h Z\Theta_c + b_0 S_{Af}, \quad (4)$$

and

$$\rho'_N(Z) = -\frac{C_b}{2}(\Theta_w - \Theta_0)^2 - T_h Z\Theta_w + b_0 S_{As}. \quad (5)$$

The respective temperature and salinity differences between the two regions are

$$\Delta\Theta = \Theta_c - \Theta_w, \quad \Delta S_A = S_{Af} - S_{As}. \quad (6)$$

The density difference at Z is

$$\Delta\rho(Z) = \rho'_S(Z) - \rho'_N(Z), \quad (7)$$

which from Eqs. (4) and (5) reduce to

$$\Delta\rho(Z) = -\frac{C_b}{2}\Delta\Theta[(\Theta_c - \Theta_0) + (\Theta_w - \Theta_0)] - T_h Z\Delta\Theta + b_0\Delta S_A. \quad (8)$$

From Eq. (8), the density difference between the regions is a linear function of the geopotential depth Z. Thus, the change in density difference arising from a change in depth from Z_1 to Z_2 can be written as

$$\Delta\rho_T = \Delta\rho(Z_1) - \Delta\rho(Z_2), \quad (9)$$

which reduces to

$$\Delta\rho_T = -T_h(Z_1 - Z_2)\Delta\Theta, \quad (10)$$

where the subscript T indicates this is a change in density difference that arises from thermobaric processes. For the case of the ocean surface ML, $Z_1 = 0$ and $Z_2 = \delta$, where δ is the ML depth, giving,

$$\Delta\rho_T = T_h\delta\Delta\Theta. \quad (11)$$

Considering that this density difference due to ML thermobaricity increases linearly with depth, the ML average of this density difference increase will be half this value,

$$\Delta\rho_T = \frac{T_h}{2}\delta\Delta\Theta. \quad (12)$$

This expression implies that the extent of the ML thermobaricity depends on the ML depth and horizontal temperature difference and provides a simple estimate for the change in horizontal density difference arising from ML thermobaricity as given by the Roquet et al. (2015a) polynomial approximation. An equivalent term can be directly calculated using the TEOS-10 [Eq. (1)] as

$$\Delta\rho_T^{t10} = \frac{\Delta\rho^{t10}(\delta) - \Delta\rho^{t10}(0)}{2}, \quad (13)$$

where

$$\Delta\rho^{t10}(\delta) = \rho_S^{t10}[p(\delta)] - \rho_N^{t10}[p(\delta)],$$
$$\Delta\rho^{t10}(0) = \rho_S^{t10}[p(0)] - \rho_N^{t10}[p(0)], \quad (14)$$

again with the factor of 2 reduction providing the ML average of the density difference increase due to ML thermobaric processes. Because of the nature of the TEOS-10 formulation, the individual terms responsible for ML thermobaricity are not easily separable from the complete equation of state. This is an advantage of the Roquet et al. (2015a) polynomial where the thermobaric influence on ML density can be simply expressed by the ML depth and temperature fields [Eq. (12)]. The comparison of the $\Delta\rho_T$ estimate from Eq. (12) with that calculated directly from the TEOS-10 serves as an evaluation of the ML thermobaric representation in the Roquet et al. (2015a) approximation.

Equation (3) can also be used to estimate the increase in the ML density difference due to cabbeling effects. For this estimate, we seek the difference between the density of the mean temperature and salinity and the average density of the two regions. The mean temperature Θ_m and salinity S_{Am} are given by

$$\Theta_m = \frac{\Theta_c + \Theta_w}{2}, \quad S_{Am} = \frac{S_{Af} + S_{As}}{2}, \quad (15)$$

and the density anomaly ρ'_m of this mean product is

$$\rho'_m(Z) = -\frac{C_b}{2}(\Theta_m - \Theta_0)^2 - T_h Z\Theta_m + b_0 S_{Am}. \quad (16)$$

The change in the density difference arising from cabbeling effects at geopotential Z is

$$\Delta\rho_C(Z) = \rho'_m(Z) - \frac{[\rho'_S(Z) + \rho'_N(Z)]}{2}, \quad (17)$$

where the subscript C indicates this is a change in density difference that arises from cabbeling processes. Using Eqs. (4)–(6), (15), and (16), the change in density difference due to ML cabbeling reduces to

$$\Delta\rho_C = \frac{C_b}{8}(\Delta\Theta)^2, \tag{18}$$

where the terms relating to Z cancel. That is, according to the Roquet et al. (2015a) polynomial approximation, the increase in density difference due to cabbeling processes is independent of depth. Note that this estimate for the increase in the density difference due to ML cabbeling is an upper bound, as it assumes the source waters are mixed in equal volumes. It also suggests the extent of ML cabbeling is primarily a function of the temperature difference alone.

The TEOS-10 can also be used to directly calculate the ML cabbeling, $\Delta\rho_C^{t10}$, by

$$\Delta\rho_C^{t10}[p(0,\delta)] = \rho_m^{t10}[p(0,\delta)] - \left\{\frac{\rho_S^{t10}[p(0,\delta)] + \rho_N^{t10}[p(0,\delta)]}{2}\right\}. \tag{19}$$

Note that this term is approximately insensitive to the pressure at which it is calculated {i.e., $\Delta\rho_C^{t10}[p(0)] \approx \Delta\rho_C^{t10}[p(\delta)]$}, and so hereinafter we use $p(0)$. This local density difference increase due to ML cabbeling uses the average of the source temperatures and salinities and is therefore the largest difference possible, giving an upper bound to the potential influence of ML cabbeling. As in the case of ML thermobaricity, the individual terms responsible for ML cabbeling are not separable in the complete equation of state, meaning there is not a simple expression for the effect of ML cabbeling from TEOS-10, unlike the Roquet et al. (2015a) polynomial. Again, the comparison of the $\Delta\rho_C$ estimate from the Roquet et al. (2015a) approximation and that calculated directly with the TEOS-10 provides an evaluation of the former.

It is interesting to note that the estimates for ML thermobaricity and ML cabbeling developed with the Roquet et al. (2015a) polynomial approximation are both independent of salinity. This does not mean that salinity is irrelevant to these processes in the ML. For instance, both processes are influenced by temperature differences, which can be enhanced by the presence of a density-compensating salinity field that maintains the dynamical stability of the temperature front. In this way the ML thermobaricity and ML cabbeling can be thought of as being indirectly dependent on the salinity field, through its ability to sustain and enhance temperature fronts.

From Eq. (10) it is clear that the change in density difference due to ML thermobaricity changes sign for an increase or decrease in depth; increasing the pressure by sinking the waters will increase the density difference, while shoaling the waters will reduce the density difference. For ML cabbeling, however, Eq. (18) highlights that the change in density difference is positive definite. Equations (12) and (18) and Eqs. (13) and (19) provide the means to investigate the extent to which these processes influence the ML density field.

Using the Roquet et al. (2015a) polynomial, we define the ML cabbeling–thermobaricity number CT_{ML} as the nondimensional ratio of Eqs. (18) and (12),

$$CT_{\mathrm{ML}} = \frac{C_b|\Delta\Theta|}{4T_h\delta}. \tag{20}$$

The number CT_{ML} is an indicator for where the Roquet et al. (2015a) approximation suggests ML cabbeling or ML thermobaricity are locally dominant in the ML. For $CT_{\mathrm{ML}} > 1$ the density difference increase due to ML cabbeling is larger than that due to ML thermobaricity; for $CT_{\mathrm{ML}} < 1$, the change in density difference due to ML thermobaricity is larger than that of ML cabbeling. The ML cabbeling–thermobaricity number can also be calculated directly from the TEOS-10 as

$$CT_{\mathrm{ML}}^{t10} = \frac{\Delta\rho_C^{t10}}{\Delta\rho_T^{t10}}. \tag{21}$$

Again, the TEOS-10 formulation means a simple expression for CT_{ML}^{t10} is not possible, and Eq. (20) can serve as an approximation.

The changes in density difference due to ML thermobaricity and ML cabbeling can be put into context by comparing these changes with the dynamic density difference already present at the surface [$\Delta\rho_0$ from Eq. (8) with $Z = 0$]. For this we define the normalized indices R_T and R_C for ML thermobaricity and ML cabbeling, respectively, as

$$R_T = \frac{|\Delta\rho_T|}{|\Delta\rho_T| + |\Delta\rho_0|}, \quad R_C = \frac{\Delta\rho_C}{\Delta\rho_C + |\Delta\rho_0|}. \tag{22}$$

These indices span the range [0, 1]. For values close to 0, the change in the density difference due to the respective nonlinear process is dynamically weak; for R_T, $R_C \to 1$ these nonlinear processes are strong. Given that ML thermobaricity and ML cabbeling are not mutually exclusive, it is useful to define a third index R_T^C to indicate the relative contributions of the two processes as

$$R_T^C = \frac{\Delta\rho_C - |\Delta\rho_T|}{\Delta\rho_C + |\Delta\rho_T| + |\Delta\rho_0|}. \tag{23}$$

The index R_T^C spans [−1, 1]; for values close to 1 (−1), the increase in the density difference arising from ML cabbeling (thermobaricity) is dominant.

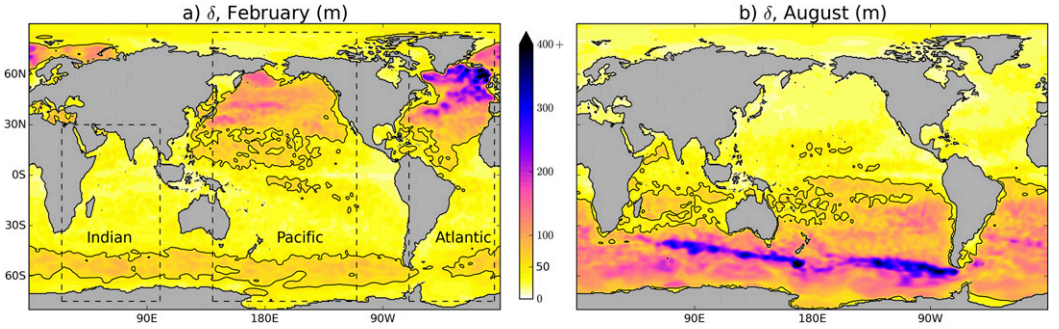

FIG. 2. MIMOC ML depth δ for (a) February and (b) August, with the $\delta = 50$ m contoured in black. The dashed regions are those used in Fig. 6.

Equivalent indices R_T^{t10}, R_C^{t10}, and R_{CT}^{t10} can be defined using TEOS-10 as

$$R_T^{t10} = \frac{|\Delta\rho_T^{t10}|}{|\Delta\rho_T^{t10}| + |\Delta\rho_0^{t10}|}, \quad R_C^{t10} = \frac{\Delta\rho_C^{t10}}{\Delta\rho_C^{t10} + |\Delta\rho_0^{t10}|}, \tag{24}$$

and

$$R_{CT}^{t10} = \frac{\Delta\rho_C^{t10} - |\Delta\rho_T^{t10}|}{\Delta\rho_C^{t10} + |\Delta\rho_T^{t10}| + |\Delta\rho_0^{t10}|}, \tag{25}$$

allowing for a direct comparison with those calculated using the Roquet et al. (2015a) polynomial approximation [Eqs. (22) and (23)].

3. Data and methodology

Determining the extents of ML cabbeling and ML thermobaricity requires knowledge of the ML temperature, salinity, and depth. For this we employ the MIMOC product (Schmidtko et al. 2013). This is a monthly climatology of ML Conservative Temperature Θ, Absolute Salinity S_A, and maximum pressure p (or equivalent ML depth δ; Fig. 2) on a 0.5° × 0.5° global grid. The MIMOC product is developed using all available quality-controlled hydrographic profiles of conductivity–temperature–depth instruments from the Argo Program (Roemmich et al. 2009), Ice-Tethered Profiles (Toole et al. 2011), and archived in the World Ocean Database (Boyer et al. 2009) for the period circa 2007–11. The data are obtained from the NOAA website (http://www.pmel.noaa.gov/mimoc/).

To estimate the ML cabbeling and ML thermobaricity, we use the ML depth and maximum local temperature differences of the MIMOC product. This methodology provides oceanographically relevant temperatures and its spatial variability at length scales appropriate for ML dynamics. The maximum local temperature difference is defined as the maximum absolute temperature difference between a given point and its neighbors,

$$\Delta\Theta(i,j) = \max|\Theta(i,j) - \Theta([i-1:i+1],[j-1:j+1])|, \tag{26}$$

where (i, j) are the longitudinal and latitudinal indices, respectively. The neighboring point that provides this maximum temperature difference is referred to as the neighboring point of interest[3] (subscript npoi). Considering the 0.5° horizontal resolution of the MIMOC product, the ML depth δ may vary appreciably between a given point and its neighboring point of interest. To account for this possible difference in ML depths, Eqs. (12) and (18) are recalculated with the depths δ and δ_{npoi}, giving,

$$\Delta\rho_T = \frac{T_h}{2}\Delta\Theta\frac{(\delta + \delta_{\text{npoi}})}{2} \le \frac{T_h}{2}\delta\Delta\Theta, \tag{27}$$

and

$$\Delta\rho_C = \frac{C_b}{2}(\Delta\Theta)^2\frac{(\delta\delta_{\text{npoi}})}{(\delta + \delta_{\text{npoi}})^2} \le \frac{C_b}{8}(\Delta\Theta)^2, \tag{28}$$

respectively. For $\delta = \delta_{\text{npoi}}$, Eqs. (27) and (28) simplify to Eqs. (12) and (18), respectively, which serve as upper limits of the extent to which ML thermobaricity and ML cabbeling influence the ML density field. The difference between the local density ρ_0 and that of the neighboring point of interest $\rho_{0,\text{npoi}}$ gives the local dynamic density difference $\Delta\rho_0 = |\rho_0 - \rho_{0,\text{npoi}}|$, and subsequently the normalized indices R_T, R_C, and R_T^C [Eqs. (22) and (23)].

We also employ the TEOS-10 and associated Python software packages (IOC et al. 2010) to directly calculate

[3] The results were largely insensitive to a widening of the search area to include second and third neighbors.

the density fields for the ocean surface ρ_0^{t10} and bottom of the ML ρ_δ^{t10} [Eq. (1)]. Again, the maximum local temperature difference is used to identify the neighboring point of interest, which is subsequently used to calculate the local density difference fields for the ocean surface $\Delta\rho_0^{t10} = |\rho_0^{t10} - \rho_{0,\mathrm{npoi}}^{t10}|$ and the bottom of the ML $\Delta\rho_\delta^{t10} = |\rho_\delta^{t10} - \rho_{\delta,\mathrm{npoi}}^{t10}|$. These density differences are used with Eq. (13) to directly calculate the change in local average ML density difference due to ML thermobaricity, $\Delta\rho_T^{t10} = (\Delta\rho_\delta^{t10} - \Delta\rho_0^{t10})/2$.

To calculate the local ML density difference increase arising from ML cabbeling, we first calculate the average temperature $\overline{\Theta}$ and salinity $\overline{S_\mathrm{A}}$ of each point and its neighboring point of interest, which would be the temperatures and salinities of the evenly mixed product. The density of this surface mixed water is

$$\rho_{\overline{\Theta}\,\overline{S_\mathrm{A}}0}^{t10} = \rho[\overline{\Theta}, \overline{S_\mathrm{A}}, p(0)]. \tag{29}$$

Using Eq. (19), the local density difference increase due to ML cabbeling is given by the difference between the density of the evenly mixed product and the average density of the local (ρ_0^{t10}) and neighboring point of interest ($\rho_{0,\mathrm{npoi}}^{t10}$),

$$\Delta\rho_C^{t10} = \rho_{\overline{\Theta}\,\overline{S_\mathrm{A}}0}^{t10} - \frac{(\rho_0^{t10} + \rho_{0,\mathrm{npoi}}^{t10})}{2}. \tag{30}$$

Here, we estimate the extent to which ML cabbeling and ML thermobaricity influence the ML density field in the MIMOC product using the simplified expressions developed from Roquet et al. (2015a) [Eqs. (12) and (18)], and calculate it directly using the TEOS-10 [Eqs. (13) and (19)]. Considering the seasonality of the ML depth δ and its influence on these terms, particularly those relating to thermobaric processes, we focus our analysis on the February and August climatologies as these represent the austral and boreal seasonal extremes.

4. Results and discussion

The spatial distribution of the MIMOC ML depth δ is predominantly basin scale and overlain with smooth, $O(10^2$–$10^3)$ km regional variability (Fig. 2). The seasonality of δ is substantial, particularly for subpolar regions where the winter ML reaches depths of over 400 m in the South Pacific and North Atlantic Oceans. The MIMOC ML depth is shallowest in the equatorial and polar regions, especially during summer, typically less than 50 m (contoured in Fig. 2).

The distribution of the extent to which ML cabbeling increases the local ML density differences $\Delta\rho_C$ is dominated by intense localized zonally coherent features in regions known for strong fronts, such as the Antarctic Circumpolar Current (ACC) and Kuroshio and Gulf Stream Extensions (Figs. 3a,b). The $\Delta\rho_C$ is smallest in the tropics (except for the equatorial eastern Pacific) and polar oceans where the horizontal gradients of ML temperature are small. The strongest features of the $\Delta\rho_C$ distribution are perennial.

The extent of the change in local density difference due to ML thermobaricity $\Delta\rho_T$ exhibits a relatively broader distribution and stronger seasonality (Figs. 3c,d) compared with that of $\Delta\rho_C$. The effect of ML thermobaricity is strongest in winter, although the general distribution is present year-round. The regions that exhibit the largest values of $\Delta\rho_C$ (ACC and Kuroshio and Gulf Stream Extensions) also have strong wintertime $\Delta\rho_T$.

Figures 3e and 3f depict the distributions of CT_ML [from Eq. (20)], providing a means to visualize the relative extents of ML cabbeling and ML thermobaricity. The CT_ML number is less than 1 (shown in blue) where the extent of ML thermobaricity is larger than that of ML cabbeling, and greater than 1 (red) vice versa. Globally, the extent of ML thermobaricity is larger than that of ML cabbeling in the MIMOC product. The ML cabbeling–thermobaricity comparison exhibits substantial seasonality, showing ML cabbeling to be more dominant during summer. Of particular note is the Kuroshio and Gulf Stream Currents and Extensions, where the extent of ML cabbeling is larger than ML thermobaricity year-round.

The spatial distributions of $\Delta\rho_C$, $\Delta\rho_T$, and CT_ML shown in Fig. 3 provide an opportunity to evaluate the estimates developed with the Roquet et al. (2015a) approximation against those calculated directly from TEOS-10 [Eqs. (13), (19), and (20)]. For the ML density difference fields (Figs. 3a–d), the respective $\Delta\rho_C^{t10}$, $\Delta\rho_T^{t10} = \pm 1.5 \times 10^{-3}$ kg m^{-3} contours are included in cyan. These exhibit exceptional spatial agreement with the simple estimates of the Roquet et al. (2015a) approximation, and the seasonality is well represented. The distributions of CT_ML also indicate good spatial agreement between the two methodologies (Figs. 3e,f; $CT_\mathrm{ML}^{t10} = 0.1, 1.9$; contoured in black). These comparisons suggest the locations and spatial distributions of the extent of ML thermobaricity and ML cabbeling are well represented by the simple estimates of the Roquet et al. (2015a) polynomial approximation.

The extent to which ML cabbeling and ML thermobaricity influence the ML density field can be put into context when normalized by the existing dynamic ML density differences, as R_C, R_T, and R_T^C [Eqs. (22) and (23)]. The normalized increase due to ML cabbeling R_C

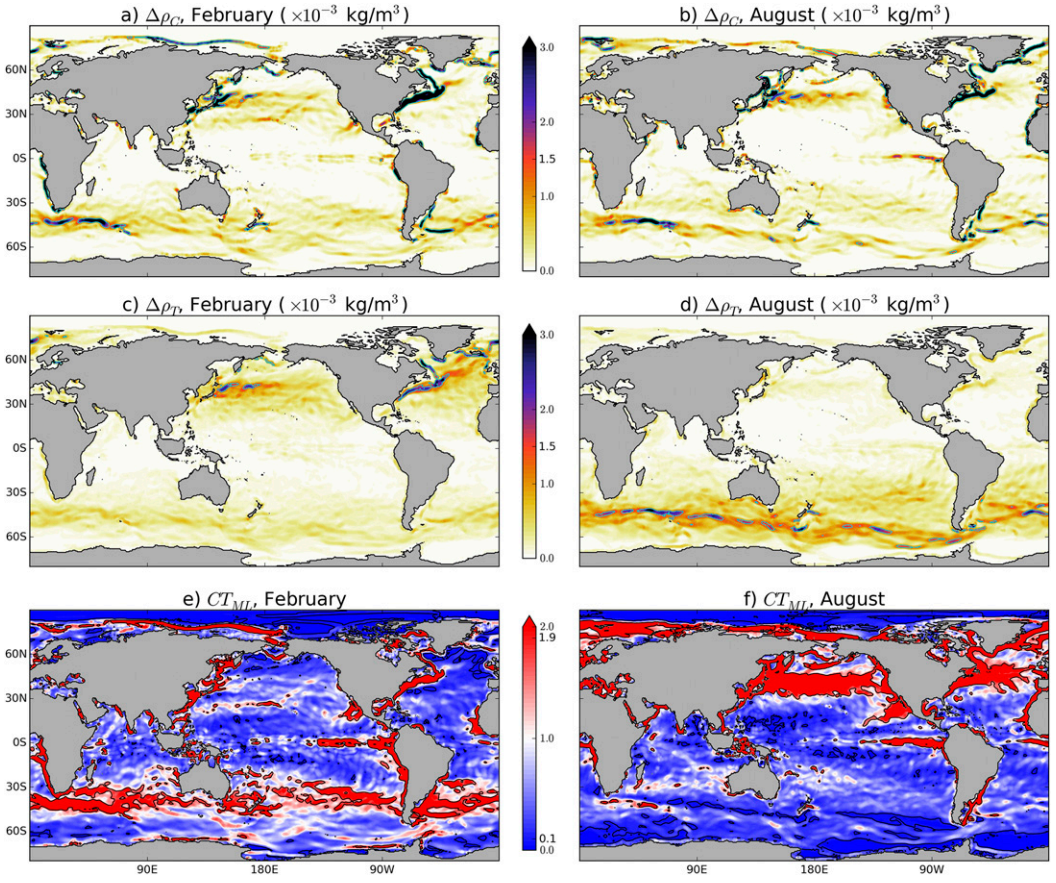

FIG. 3. The extent to which (a),(b) ML cabbeling and (c),(d) ML thermobaricity can increase the local ML horizontal density difference as estimated by the Roquet et al. (2015a) polynomial approximation. The $\Delta\rho^{t10} = \pm 1.5 \times 10^{-3}$ kg m^{-3} values calculated using the TEOS-10 are contoured in cyan. (e),(f) The relative contributions of ML cabbeling and ML thermobaricity can be visualized by the distribution of the ML cabbeling–thermobaricity number CT_{ML}, where the $CT_{\mathrm{ML}}^{t10} = 0.1$, 1.9 values are contoured in black.

exhibits more seasonality than the $\Delta\rho_C$ field (cf. Figs. 3a,b with Figs. 4a,b). The zonally coherent regions of strong ML cabbeling remain evident, although low-latitude normalized cabbeling is weak. For ML thermobaricity, the normalized increase R_T is zonally broader than the $\Delta\rho_T$ fields but confined to latitudes poleward of 30° (Figs. 4c,d). The seasonality in the normalized ML thermobaricity extent remains strong, with the largest effect during winter. The normalized relative extents R_T^C also exhibits a poleward concentration (Figs. 4e,f); the effects of ML cabbeling and ML thermobaricity are strongest at latitudes poleward of 30° in both hemispheres. The contribution from ML thermobaricity is basin-scale and largest in winter. The contribution from ML cabbeling is confined to zonally coherent regions of strong fronts and is largest in summer, except for the Gulf Stream, Kuroshio, and Kerguelen Plateau regions, where it dominates year-round.

Again, the normalized indices depicted in Fig. 4 allow comparisons to be made between the estimates of the Roquet et al. (2015a) approximation and the TEOS-10. In each panel the ±4% contour of the TEOS-10 indices [Eqs. (24) and (25)] are included, highlighting the good spatial agreement between the fields. A more direct comparison of the indices is the two-dimensional histograms shown in Fig. 5. The latitudinal influence on these indices is highlighted by the colored contours indicating the 95% thresholds (5% of those regions exist outside these contours); cyan are poleward of 60°, green are between 30° and 60°, and magenta are equatorward of 30°. The normalized density difference increases due to ML cabbeling calculated with the Roquet et al. (2015a) polynomial, and the TEOS-10 have correlation coefficients of 0.57 and 0.5 for February and August, respectively (Figs. 5a,b). These correlations are smaller than those for ML thermobaricity, which are 0.76 and 0.81 for February and August, respectively (Figs. 5c,d).

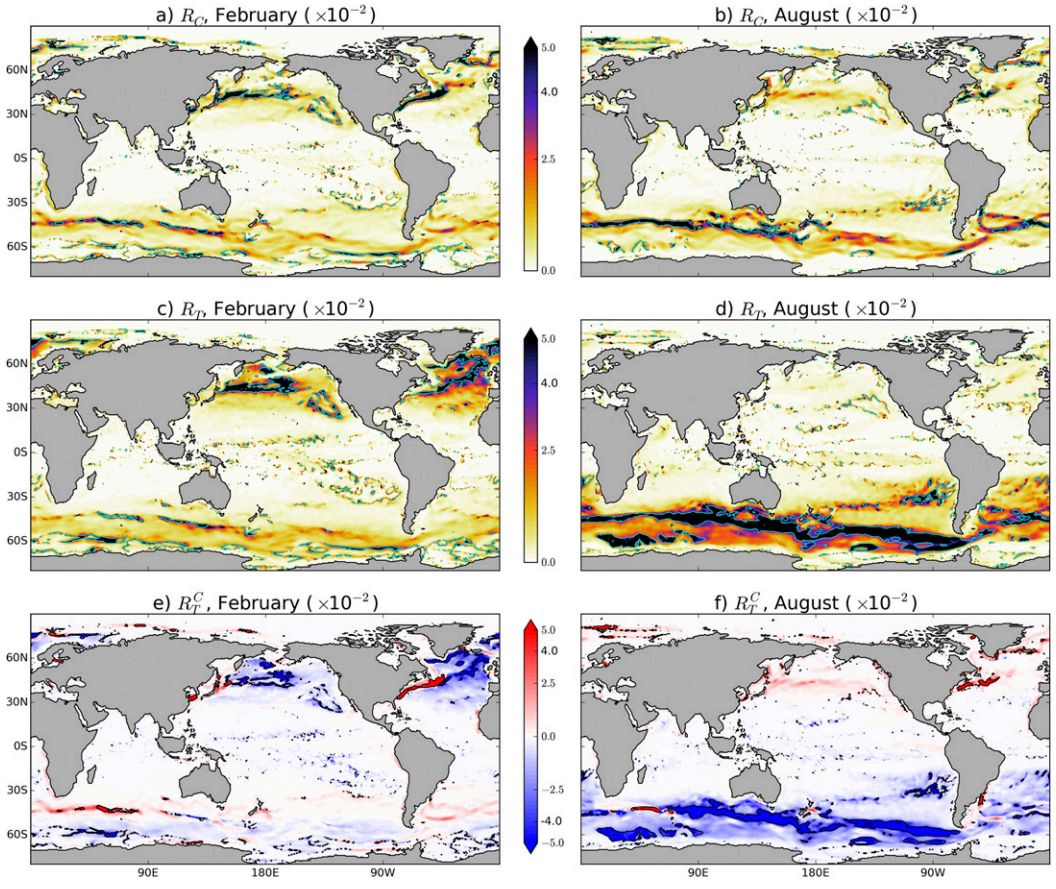

FIG. 4. The normalized indices (a),(b) R_C; (c),(d) R_T; and (e),(f) R_T^C calculated using the Roquet et al. (2015a) polynomial. The respective ± 0.04 value of the TEOS-10 indices are contoured in cyan in (a)–(d) and in black in (e) and (f).

The difference between these correlations for ML cabbeling and ML thermobaricity indicate that the representation of ML thermobaricity in the Roquet et al. (2015a) polynomial is more accurate than that of ML cabbeling. That is, Eq. (27) is a better approximation of ML thermobaricity than Eq. (28) is for ML cabbeling, which presumably reflects the relative thermodynamic complexities of the two processes. The normalized relative contributions (R_T^C and R_{CT}^{t10}; Figs. 5e,f) exhibit stronger correlations (0.81 and 0.85 for February and August, respectively) than the normalized indices for either ML cabbeling or ML thermobaricity. Note that the histogram data exist almost exclusively in the upper-right or lower-left quadrant, which is indicative of the ability of the Roquet et al. (2015a) approximation to predict the relative extents of the ML cabbeling and ML thermobaricity.

The zonal coherency of these ML features is worth investigating. For this we partition the ocean into the Indian, Pacific, and Atlantic sectors (outlined in Fig. 2a), and calculate the zonal averages of the normalized indices R_C and R_T (Fig. 6). This analysis highlights the poleward concentration of these terms to latitudes greater than 30°. It also demonstrates their seasonality, especially the winter intensification of ML thermobaricity. The peaks of the ML thermobaricity indices are broader than those of ML cabbeling, indicative of the latter's localized distribution. During the austral winter, ML thermobaricity is responsible for upward of 5% of the local density difference between 40° and 60°S, with latitudes in the Pacific and Indian sectors reaching over 10% and 25%, respectively. Equivalent broad swathes of $R_T > 5\%$ are present in the boreal winter between 40° and 50°N, and extending northward of 60°N in the Atlantic sector. The equivalent zonal averages of the normalized indices calculated with the TEOS-10 (dashed lines of Fig. 6) indicate good agreement with the Roquet et al. (2015a) approximation, although the latter tends to slightly overestimate the relative extent of ML thermobaricity in the Southern Ocean.

The Roquet et al. (2015a) polynomial for estimating ML cabbeling and ML thermobaricity relies on the prescribed, globally constant coefficients T_h and C_b,

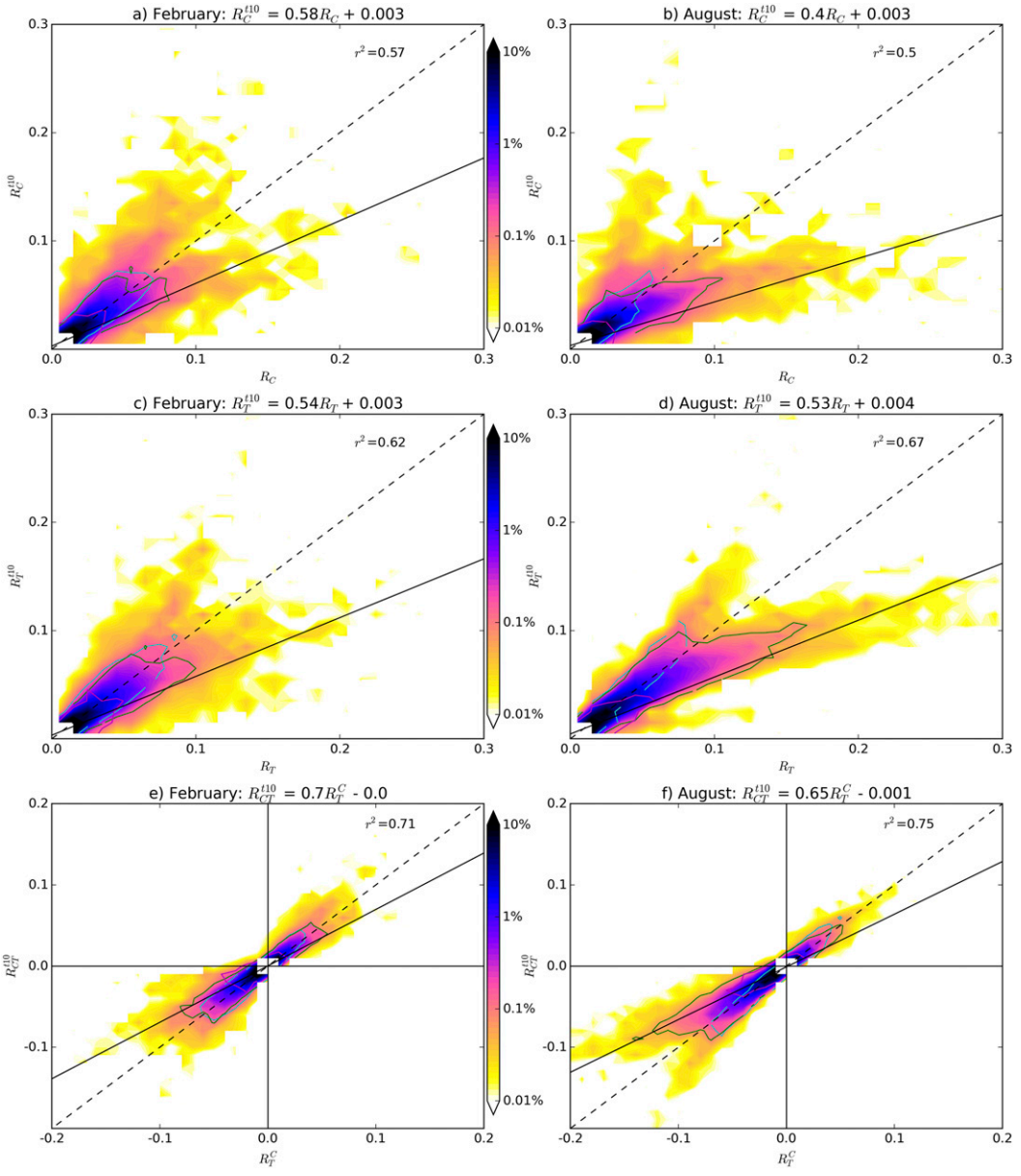

FIG. 5. Two-dimensional histograms comparing the normalized indices (a),(b) R_C; (c),(d) R_T; and (e),(f) R_T^C calculated using the Roquet et al. (2015a) approximation with those calculated using the TEOS-10 (R_C^{t10}, R_T^{t10}, and R_{CT}^{t10}). The contours indicate the 95% thresholds for three latitudinal bands; cyan is poleward of 60°, green is between 30° and 60°, and magenta is equatorward of 30°. The formulas for the lines of best fit (shown in solid black) are given in the figure title, and the correlation coefficient shown in the upper right.

respectively. The values of these coefficients can be independently evaluated for the ML by combining Eqs. (12) and (13) for T_h and Eqs. (18) and (19) for C_b, as

$$T_h^{t10} = \frac{2\Delta\rho_T^{t10}}{\delta\Delta\Theta}, \quad C_b^{t10} = \frac{8\Delta\rho_C^{t10}}{(\Delta\Theta)^2}. \tag{31}$$

Here, T_h^{t10} and C_b^{t10} are spatially variable fields for which T_h and C_b are constant approximations. It is useful to compare these fields to their respective constant approximations by their normalized differences, $(T_h^{t10} - T_h)/T_h$ and $(C_b^{t10} - C_b)/C_b$. Note that the coefficients T_h and C_b are selected to be globally representative and that the wide range of temperatures in the ML serves as a challenging test. Figure 7 depicts these normalized differences; for regions less than 0 (blue), the T_h or C_b constant approximation (and

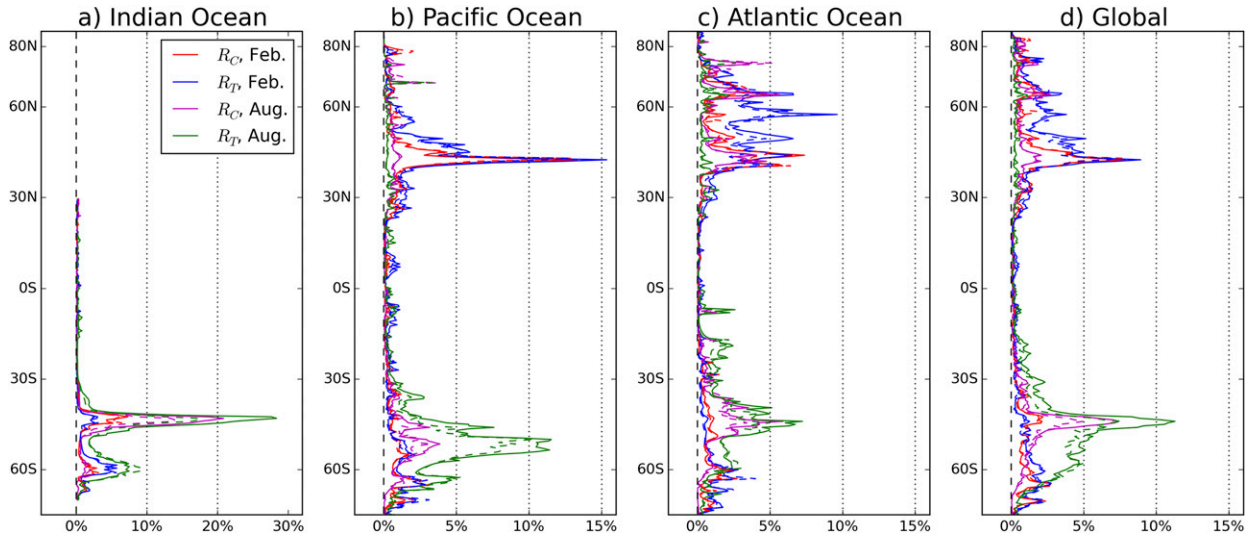

FIG. 6. The zonal averages of the normalized indices R_C (red, magenta) and R_T (blue, green) for the (a) Indian, (b) Pacific, and (c) Atlantic Ocean sectors and (d) the global average. The equivalent values for the normalized indices calculate with the TEOS-10 (R_C^{t10} and R_T^{t10}) are indicated by the dashed lines. The sector boundaries are shown in Fig. 2a.

subsequent ML thermobaricity or ML cabbeling extent estimate) is too large, and for regions greater than 0 (red) vice versa. The color scale saturates at ±1, where the difference between the evaluated coefficient and the constant coefficient becomes greater than the latter.

For ML thermobaricity, >92.5% of the MIMOC global area has T_h^{t10} within ±100% of T_h, with >71.9% area within ±50% of T_h (contoured in Figs. 7a,b). For ML cabbeling, >91.7% of the global area has C_b^{t10} within ±100% of C_b, with >83.8% area within ±50% of C_b (contoured in Figs. 7c,d). In general, the C_b and T_h coefficients tend to overestimate the extent of ML cabbeling and ML thermobaricity in the equatorial and tropical latitudes and underestimate them in the subpolar regions. The distributions in Fig. 7 indicate that T_h^{t10} and C_b^{t10} are (weak) functions of temperature.

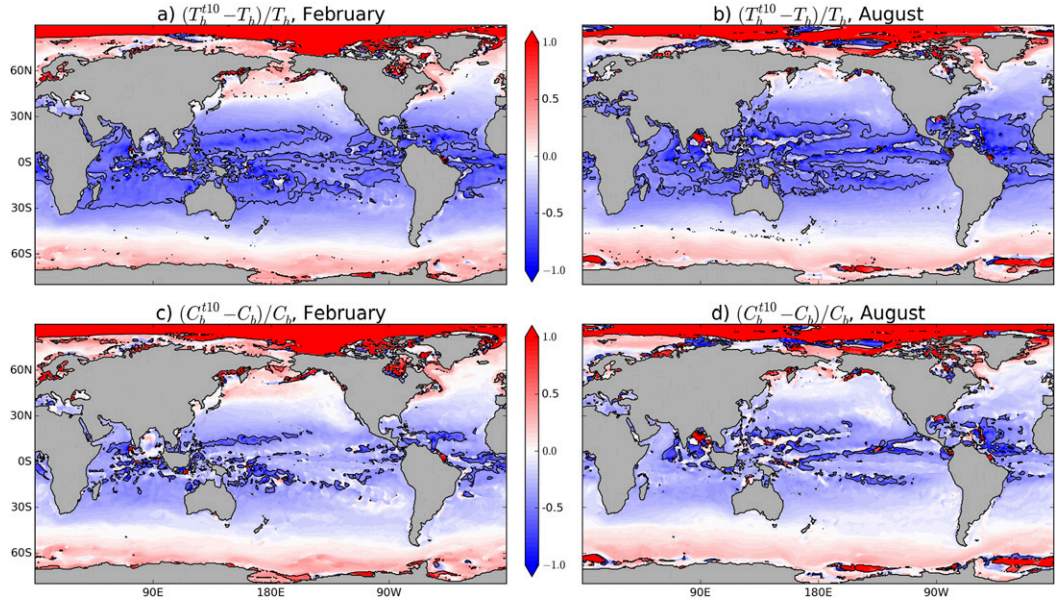

FIG. 7. Distributions of the evaluated (a),(b) thermobaric and (c),(d) cabbeling coefficients compared with their respective prescribed constants. The ±50% contours are shown in black.

5. Conclusions

The influence of cabbeling and thermobaric processes on the ML density field has been estimated using the local temperature difference and ML depth with the Roquet et al. (2015a) polynomial approximation, and calculated directly using the TEOS-10. Traditional methods to investigate these processes are ill suited to examine the ML, requiring a new approach developed specifically to accommodate ML dynamics and the underlying thermodynamics of cabbeling and thermobaricity. Here, the effects of ML thermobaricity are expressed in terms of an increase in the local ML horizontal density difference resulting from the increase in pressure through the ML. The effects of ML cabbeling are given in terms of the difference between the product water density and average density of the source waters following a mixing of neighboring water masses. Both of these effects, arising from different processes that are ubiquitous throughout the ML, provide a source of available potential energy at density-compensated ML fronts, thus acting to deepen the ML and facilitate mode water formation (e.g., Thomas and Shakespeare 2015).

We find ML thermobaricity and ML cabbeling predominantly occur poleward of 30°. When compared in terms of their influence on local ML density difference, the extent of ML thermobaricity is basin scale, winter intensified, and generally larger than that of ML cabbeling. Mixed layer cabbeling is typically perennial and localized to intense zonally coherent regions associated with strong temperature fronts (ACC and Kuroshio and Gulf Stream Extensions), regions where ML cabbeling is always stronger than that of ML thermobaricity. The extent of ML cabbeling and thermobaricity can reach up to a fifth of the local ML density difference. The simple analytical methodology for estimating the extent of ML cabbeling and ML thermobaricity compares well with the direct calculation using the full TEOS-10.

This study highlights the importance of employing an appropriate equation of state in ocean models, especially for global and high-latitude simulations. These findings demonstrate the sensitivity of the effects of 1) ML thermobaricity to the ML depth and 2) ML cabbeling to ML temperature gradients. An ocean model that chronically over- or underestimates the ML depth will misrepresent the extent to which ML thermobaricity densifies the ML. Additionally, an ocean model that actively smooths or sharpens ML temperature gradients will influence the extent of ML cabbeling. These effects are sensitive to model resolution and will be further enhanced as submesoscale structures are better represented. Nevertheless, these nonlinear equation-of-state dynamics must be accommodated as ocean models continue improving and implementing sophisticated ML and submesoscale schemes.

Acknowledgments. The Monthly Isopycnal/Mixed-Layer Ocean Climatology (MIMOC) product of Schmidtko et al. (2013) was sourced from the NOAA website (http://www.pmel.noaa.gov/mimoc/) downloaded 12 December 2016. Many thanks to R. W. Griffiths, A. Klocker, T. McDougall, and C. Shakespeare for very helpful discussions. K.D.S. was supported by Australian Research Council Grant DP140103706; T.W.N.H. was supported by National Science Foundation Grants 1338814 and 1536554, and A.M.H. was supported by Australian Research Council Grant CE110001028. The authors thank the two anonymous reviewers for their valuable comments and suggestions to improve the quality of the paper.

REFERENCES

Boyer, T. P., and Coauthors, 2009: World Ocean Database 2009. S. Levitus, Ed., NOAA Atlas NESDIS 66, 216 pp.

Carmack, E. C., 2007: The alpha/beta ocean distinction: A perspective on freshwater fluxes, convection, nutrients and productivity in high-latitude seas. *Deep-Sea Res. II*, **54**, 2578–2598, doi:10.1016/j.dsr2.2007.08.018.

Groeskamp, S., R. P. Abernathey, and A. Klocker, 2016: Water mass transformation by cabbeling and thermobaricity. *Geophys. Res. Lett.*, **43**, 10 835–10 845, doi:10.1002/2016GL070860.

Haine, T. W. N., and J. Marshall, 1998: Gravitational, symmetric, and baroclinic instability of the ocean mixed layer. *J. Phys. Oceanogr.*, **28**, 634–658, doi:10.1175/1520-0485(1998)028<0634:GSABIO>2.0.CO;2.

IOC, SCOR, and IAPSO, 2010: *The International Thermodynamic Equation of Seawater—2010: Calculation and Use of Thermodynamic Properties*. Intergovernmental Oceanographic Commission Manuals and Guides, No. 56, UNESCO, 196 pp. [Available online at http://www.teos-10.org/pubs/TEOS-10_Manual.pdf.]

Klocker, A., and T. J. McDougall, 2010: Influence of the nonlinear equation of state on global estimates of dianeutral advection and diffusion. *J. Phys. Oceanogr.*, **40**, 1690–1709, doi:10.1175/2010JPO4303.1.

McDougall, T. J., 1987: Thermobaricity, cabbeling, and water-mass conversion. *J. Geophys. Res.*, **92**, 5448–5464, doi:10.1029/JC092iC05p05448.

Nycander, J., M. Hieronymus, and F. Roquet, 2015: The nonlinear equation of state of sea water and the global water mass distribution. *Geophys. Res. Lett.*, **42**, 7714–7721, doi:10.1002/2015GL065525.

Roemmich, D., and Coauthors, 2009: The Argo program: Observing the global ocean with profiling floats. *Oceanography*, **22**, 34–43, doi:10.5670/oceanog.2009.36.

Roquet, F., G. Madec, L. Brodeau, and J. Nycander, 2015a: Defining a simplified yet "realistic" equation of state for

seawater. *J. Phys. Oceanogr.*, **45**, 2564–2579, doi:10.1175/JPO-D-15-0080.1.

——, ——, T. J. McDougall, and P. M. Barker, 2015b: Accurate polynomial expressions for the density and specific volume of seawater using the TEOS-10 standard. *Ocean Modell.*, **90**, 29–43, doi:10.1016/j.ocemod.2015.04.002.

Schmidtko, S., G. C. Johnson, and J. M. Lyman, 2013: MIMOC: A global monthly isopycnal upper-ocean climatology with mixed layers. *J. Geophys. Res. Oceans*, **118**, 1658–1672, doi:10.1002/jgrc.20122.

Stewart, K. D., and T. W. N. Haine, 2016: Thermobaricity in the transition zones between alpha and beta oceans. *J. Phys. Oceanogr.*, **46**, 1805–1821, doi:10.1175/JPO-D-16-0017.1.

Thomas, L. N., and C. J. Shakespeare, 2015: A new mechanism for mode water formation involving cabbeling and frontogenetic strain at thermohaline fronts. *J. Phys. Oceanogr.*, **45**, 2444–2456, doi:10.1175/JPO-D-15-0007.1.

Toole, J. M., R. A. Krishfield, M.-L. Timmermans, and A. Proshutinsky, 2011: The Ice-Tethered Profiler: Argo of the Arctic. *Oceanography*, **24**, 126–135, doi:10.5670/oceanog.2011.64.